Data processing and initial results from the CE-3 Extreme Ultraviolet Camera

2014 Res. Astron. Astrophys. 14 1664

(http://iopscience.iop.org/1674-4527/14/12/014)

RAA 2014 Vol. **14** No. **12**, 1664–1673 doi: 10.1088/1674–4527/14/12/014
http://www.raa-journal.org *http://www.iop.org/journals/raa*

***R**esearch in*
***A**stronomy and*
***A**strophysics*

Data processing and initial results from the CE-3 Extreme Ultraviolet Camera

Jian-Qing Feng[1], Jian-Jun Liu[1], Fei He[2], Wei Yan[1], Xin Ren[1], Xu Tan[1], Ling-Ping He[2], Bo Chen[2], Wei Zuo[1], Wei-Bin Wen[1], Yan Su[1], Yong-Liao Zou[1] and Chun-Lai Li[1]

[1] Key Laboratory of Lunar and Deep Space Exploration, National Astronomical Observatories, Chinese Academy of Sciences, Beijing, 100012, China; *liujj@nao.cas.cn*
[2] Changchun Institute of Optics, Fine Mechanics and Physics, Chinese Academy of Sciences, Changchun, 130033, China

Received 2014 July 22; accepted 2014 October 17

Abstract The Extreme Ultraviolet Camera (EUVC) onboard the Chang'e-3 (CE-3) lander is used to observe the structure and dynamics of Earth's plasmasphere from the Moon. By detecting the resonance line emission of helium ions (He^+) at 30.4 nm, the EUVC images the entire plasmasphere with a time resolution of 10 min and a spatial resolution of about 0.1 Earth radius (R_E) in a single frame. We first present details about the data processing from EUVC and the data acquisition in the commissioning phase, and then report some initial results, which reflect the basic features of the plasmasphere well. The photon count and emission intensity of EUVC are consistent with previous observations and models, which indicate that the EUVC works normally and can provide high quality data for future studies.

Key words: space vehicles: instruments: Extreme Ultraviolet Camera — Earth: plasmasphere — method: data processing

1 INTRODUCTION

The Earth's plasmasphere is a torus of low energy, dense plasma that forms a region in the Earth's inner magnetosphere, with its size being about $5 \sim 6$ Earth radii (R_E). The plasmasphere traps varieties of ions and electrons, among which He^+ ions resonantly scatter the extreme ultraviolet (EUV) radiation of sunlight at 30.4 nm and the intensity is proportional to the column density (Meier & Weller 1972; Meier 1991). The He^+ ion is the second most abundant component of the plasmasphere (Craven et al. 1997). Since the most abundant ion H^+ has no optical emission, the 30.4 nm emission is usually chosen for imaging the global plasmasphere (Carpenter 2004; Darrouzet & De Keyser 2013). In addition, since the magnetosphere is optically thin with respect to this emission (Brandt 1961) and the intensity of interplanetary background radiation is extremely low at 30.4 nm (Gruntman 1992; Jelinsky et al. 1995), the remote sensing method using EUV emission has become a powerful tool in the search for global perspectives on the structure and dynamics of the plasmasphere (Murakami et al. 2010).

In the past decades, researchers have been exploring the plasmasphere in many ways (Darrouzet & De Keyser 2013). The emergence of optical cameras with a wide field of view that can detect

the resonantly scattered sunlight at 30.4 nm has allowed space physicists to make a great progress in imaging the plasmasphere (Carpenter 2004). The first intensity distribution of partial plasmaspheric He^+ emission that was projected on the meridian plane was obtained by the X-ray ultraviolet (XUV) scanner aboard the Planet-B mission and it demonstrated that plasmaspheric EUV emission at 30.4 nm is bright enough to be taken in snapshots (Nakamura et al. 1999, 2000). A sequence of comprehensive EUV images of the plasmasphere was first carried out by the EUV imager onboard the IMAGE spacecraft (Burch 2000; Sandel et al. 2000) and many important features of the plasmasphere were observed (Adrian et al. 2001; Sandel et al. 2001, 2003; Gallagher et al. 2005). Recently, the Telescope of Extreme Ultraviolet (TEX) aboard KAGUYA conducted overall imaging of the plasmasphere from the perspective of the meridian in lunar polar orbit and observed a medium-scale density structure in the dawnside plasmasphere during a geomagnetic quiet period (2008 June 1-2) (Yoshikawa et al. 2008; Murakami et al. 2010). However, because of the limited operation period and Field of View (FoV) of the scanner, the XUV only imaged the partial plasmasphere during its near-Earth parking orbit from July 1998 to January 1999. For IMAGE EUV, the plasmasphere could only be projected into an equatorial plane and could not be imaged continuously, because IMAGE operated in a polar orbit and could only look at the Earth for half of its duty cycle. Also, because the metal band-pass filter on TEX was mechanically damaged, two circular ghosts appeared on all images, and some pixels were contaminated by the artificial structure. Therefore, the data obtained by TEX were imperfect.

The Extreme Ultraviolet Camera (EUVC) onboard the Chang'e-3 (CE-3) lander observes the Earth's plasmasphere from the perspective of the meridian. Since the spin period and the revolution period of the Moon are equal, the nearside always faces the Earth and the FoV of EUVC always points to Earth. Thus, EUVC can image the plasmasphere continuously when the Moon circles the Earth. In this paper, we introduce the data processing method used by the CE-3 EUVC and report the initial results from the first four months. The instrumentation and calibration of EUVC are summarized in Section 2. The data acquisition is presented in Section 3. Section 4 gives the steps and algorithms implemented in data processing in detail. In Sections 5, we present preliminary results and compare them with previous studies. Finally, we draw a conclusion in Section 6.

2 INSTRUMENTATION

EUVC is composed of a thin film absorption filter, an EUV multilayer mirror, a photon-counting imaging detector, a supporting mechanism, an electronic control system and a thermal control unit. In order to improve the energy transfer efficiency of the EUVC at 30.4 nm and to obtain high quality plasmaspheric images, the EUVC adopted an optical structure composed of a single spherical mirror and a spherical microchannel plate (MCP) detector. The technical parameters of the EUVC are given by Table 1.

Table 1 Technical Parameters of the EUVC

Parameter	Value
Center wavelength (nm)	30.2
Bandwidth (nm)	4.6
FoV (°)	14.7
Angular resolution (°)	0.08
Exposure time (min)	2, 10, 20
Detectable range (Rayleigh)	$0.1 \sim 10$
Sensitivity (count s^{-1} $Rayleigh^{-1}$)	$\geqslant 0.1$

The thin film absorption filter is mounted in the front of the detector to filter out emissions that can contaminate the image in ultraviolet, visible light and infrared. The 30.4 nm emissions from the plasmasphere are focused on the MCP detector through the optical system, and the incident photons

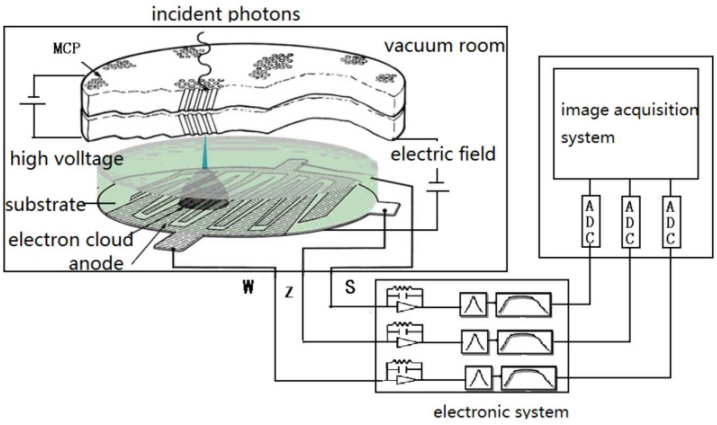

Fig. 1 Schematic diagram of the MCP detector.

that enter the MCP are transferred to photoelectrons, which are amplified by the high voltage and then ejected from the other end of the MCP. The ejected photoelectrons diffuse to an electron cloud with a certain dimension and are collected on the wedge and strip anode, which encodes the location of the centroid of the electron cloud and transfers the data to the electronics system to find the location of incident photons. Figure 1 shows the schematic diagram of the MCP detector.

The ground calibration test was performed by the EUVC instrument team at Changchun Institute of Optics, Fine Mechanics and Physics, Chinese Academy of Sciences (CIOMP, CAS) during December 2011 and October 2012 (Chen et al. 2014). The test was divided into two parts. The first part was geometric calibration which included geometric distortion, measuring the focal length and locating the image center. The second part was radiometric calibration, composed of relative radiometric calibration and absolute radiometric calibration. A Photo Response Non Uniformity matrix was measured and the sensitivity was finally given.

An original image obtained by EUVC in observation mode has 1500×1500 pixels, with each pixel value quantized into 16-bit data. The size of each image is 4.3 MB. All the pixels in the image are arranged in the form ($x1$, $y1$), ($x1$, $y2$), $\cdots$, ($x1$, $y1500$), ($x2$, $y1$), ($x2$, $y2$), $\cdots$, ($x2$, $y1500$), $\cdots$, ($x1500$, $y1$), ($x1500$, $y2$), $\cdots$, ($x1500$, $y1500$). The value of each pixel in the image represents the number of 30.4 nm photons captured by EUVC during the exposure time.

3 DATA ACQUISITION

After successfully landing on the lunar surface on 2013 December 14 (Ip et al. 2014), the instruments onboard the CE-3 lander and Yutu rover started to work. We obtained about 642 EUVC images during the first four months until the end of March 2014. In order to supply energy, the CE-3 lander and its payload had to operate during the lunar day and hibernate throughout the lunar night. Another factor taken into consideration was contamination from light. Sunlight could come into the FoV of EUVC directly at noon and reduce the quality of the images. As a result, EUVC often worked for dozens of hours in the "morning" and the "dusk" of the lunar day. The times when data were acquired during the first four months are given in Table 2.

By changing the pitch angle of the camera, EUVC alternatively imaged the "background" and "plasmasphere" during its normal operation, which meant that the EUVC took an image of the space background after taking several images of Earth's plasmasphere. The "background" images can be used to eliminate the light contamination in images of the "plasmasphere."

Table 2 Data Acquisition During the First Four Months

No	Period	Time (UTC)	Number of Images	Exposure time (min)
1	First month	2013.12.16 ∼ 2013.12.24	79	10
2	Second month	2014.01.12 ∼ 2014.01.22	177	10
3	Third month	2014.02.10 ∼ 2014.02.21	240	10
4	Fourth month	2014.03.12 ∼ 2014.03.23	146	10

4 DATA PROCESSING

The data recorded by CE-3 are received and processed by the Science and Application Center for Moon and Deep Space Exploration, affiliated with National Astronomy Observatories, Chinese Academy of Sciences (NAOC). After being extracted from the CE-3 exploration data, the EUVC raw data need a series of processing steps to generate several levels of data production including Level 1, Level 2A and Level 2B. The data from Levels 2A and 2B will be released to researchers for scientific study. The data processing flow is described in Figure 2.

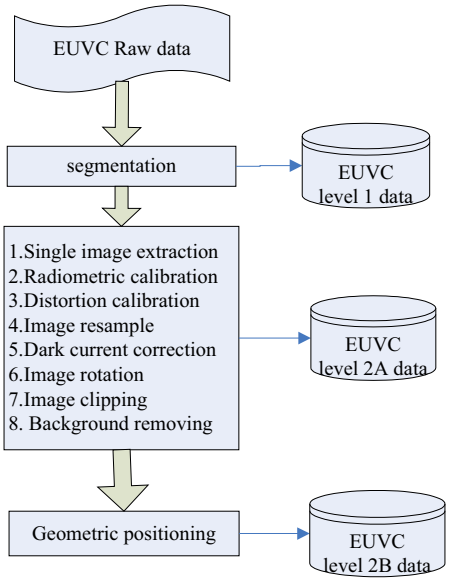

Fig. 2 EUVC data processing flow.

There is a sequence of images in EUVC raw data, so the first step is segmentation. In Level 1 data processing, the raw data are divided into several files according to the observation time, which means the images obtained during the same Earth day will be compiled into one file.

Level 2A data processing contains the following steps:

(1) Single image extraction;
(2) Radiometric calibration: multiplying the single raw image by the calibration matrix in order to eliminate the Photo Response Non-Uniformity;
(3) Distortion calibration: to eliminate the geometric distortion of the image caused by the optical system of the camera. The calibration coefficient was determined by a ground calibration test before launching;
(4) Image resampling: every set of 7×7 pixels is merged into one single pixel, and by summing their values, an image of size 214×214 will be created;

(5) Dark current correction: subtracting the dark current image from the former image;
(6) Image rotation: as there was a 60° deviation between the angle that the detector installed and the angle observations were recorded, the image has to be rotated 60° counterclockwise, using a bilinear interpolation algorithm;
(7) Image clipping: the margin of the 214 × 214 image and the irregular edge of the FoV will be cut off, with 150×150 pixels left.
(8) Background removal: this is the last step in level 2A data processing. We have to find the nearest "background" image and then subtract the product of "background" and a factor K from the "plasmasphere" image to generate a "cleaner" image.

To determine the factor K, a formula is given as

$$A_n(x,y) = A_p(x,y) - A_b(x,y) \times K \ \ (55 \leq \sqrt{(x-x_c)^2 + (y-y_c)^2} \leq 66), \tag{1}$$

where (x, y) is the pixel location and (x_c, y_c) is the center of the image. A_p and A_b represent the pixels in an annular region (55 and 66 pixels from center of the image) of the "plasmasphere" and "background" image respectively, and A_n is the result. The factor K varies from 0.05 to 5 with a stepsize of 0.025. When the mean value or standard deviation of A_n is smallest, we can get a K_M or K_S. Their average value is a reasonable factor. The steps of background removal are demonstrated in Figure 3.

Geometric positioning with Level 2B data calculates the location and pointing direction of EUVC in the solar magnetospheric system of coordinates. The positioning result is added to the Planetary Data System (PDS) label of the 2B files.

The Level 2A and Level 2B data files are produced in the PDS format, with every file consisting of a PDS label and an image. The PDS label contains essential information about the image: Image Type ("plasmasphere" or "background"), frame count, image size, working mode, beginning time, ending time, exposure time, four temperature points of the camera, azimuth angle, pitch angle and so on. Compared with 2A data, the 2B PDS label adds more information, like the positioning result. The format of the Level 2 data files is given in Table 3.

Table 3 Format of Level 2 Data

Content				Description
PDS label				PDS label contains the image information, with its length being 3600 bytes in 2A data and 4500 bytes in 2B data.
(0, 0)	(0, 1)	···	(0, 149)	The image size is 150×150×2 = 45 000 bytes with 2 bytes per pixel, little-endian.
···	···	···	···	
(149, 0)	(149, 1)	···	(149, 149)	

5 INITIAL RESULTS

Figure 4 shows a raw EUVC image taken at the last moment of the first month, without any data processing. Some large-scale structures including ionospheric airglow, and the profile and shadow of the Earth can be clearly seen. However, as a result of oversampling, the photons in the image have a uniform distribution and some plasmaspheric features cannot be recognized. In addition, the installation angle of the camera makes the Earth "rotate" at a certain angle in the image. Level 2A data processing is needed to reveal more details and address the problem mentioned above.

Figure 5 shows the result of processing Level 2A data from the raw image in Figure 4. Figure 5(a) and Figure 5(b) represent the results before and after background removal respectively. As the irregular edge of the detector is cut off in the image, the visible circular FoV is 13°. Compared with Figure 5(a), the light contamination in Figure 5(b) is substantially reduced and the profile of

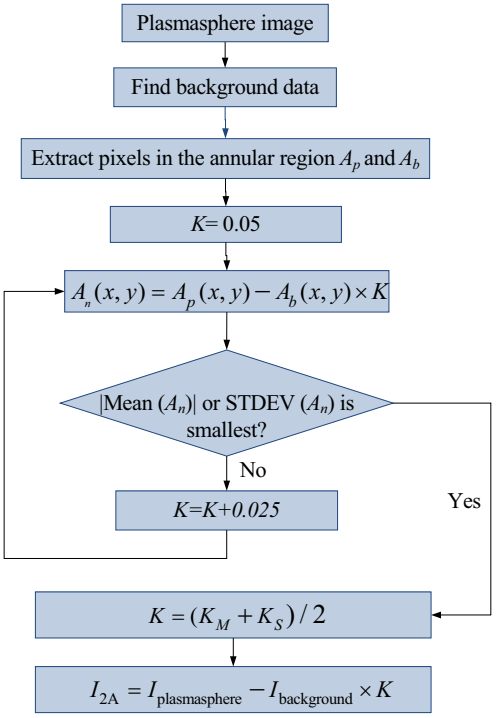

Fig. 3 The steps used in background removal. Mean(A_n) refers to the mean value of A_n and STDEV means the standard deviation. I_{2A} is the image contained in Level 2A data.

Table 4 Statistical Results of the Two Images in Figure 5

Data	Minimum	Maximum	Mean	Standard deviation
Before background removal	15	831	52.77	72.25
After background removal	0	777.34	19.78	55.86

the plasmasphere is much clearer; the average count, the minimum count and the standard deviation are smaller (listed in Table 4). The signal-to-noise ratio of the image is greatly enhanced after background removal.

We process the data recorded from the 2nd to the 4th month in the same way. Figure 6 gives some examples of the processing results. The patterns in Figures 5 and 6 show a clear plasmaspheric structure as we expect. Besides the Earth and airglow, some important features such as the plasmaspheric density profile, plume, plasmapause and even convection tail can be distinguished.

In order to characterize the data in a more general manner, we calculated the emission intensity of the images by using the following formula

$$I = \frac{\text{Pixel value}}{t \times S}, \tag{2}$$

where I is the emission intensity, t is the exposure time and S is the sensitivity determined by the ground calibration test. In this paper the value of S is 0.11 count s^{-1} Rayleigh^{-1}. Figure 7 shows the statistical results of EUVC images obtained during the first four months.

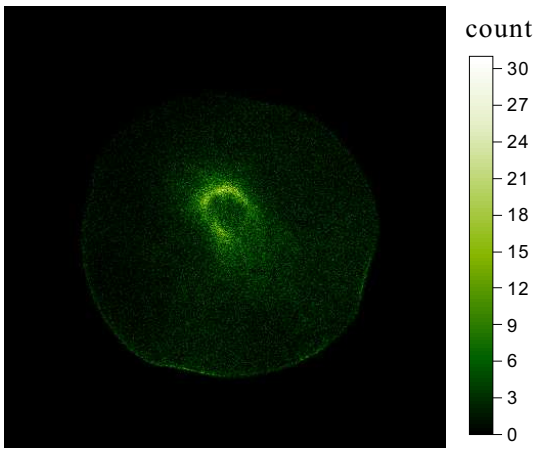

Fig. 4 A raw image obtained by CE-3 EUVC during 17:01 ∼ 17:11 on 2013 December 24 (UTC time). The size of the image is 1500 × 1500, with the color bar representing the photon count. The visible pattern in the image is the FoV of the camera; the bright area in the center is the plasmasphere.

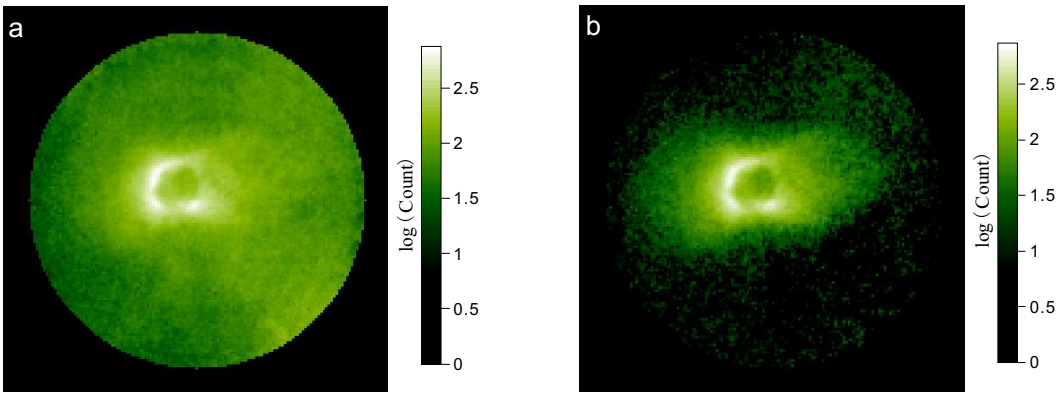

(a) (b)

Fig. 5 Two images of Level 2A data after data processing has been applied, with image size of 150×150. (a) is the image before background removal. (b) is the image after background removal. The visible FoV in the image is 13° and the angular resolution is 0.1°.

According to Figure 7, the maximal photon count of images in the first two months ranges between 500 ∼ 900 and maximal intensity ranges between 7.3 ∼ 13 Rayleigh. For the third and fourth months, however, the counts become larger, varying between 600 ∼ 3000 with maximal intensity between 8.7 ∼ 44 Rayleigh.

The intensity of Earth's plasmasphere in the EUV band was first given by people using a sounding rocket. Ogawa & Tohmatsu (1971) measured how EUV emissions of neutral helium (58.4 nm) and singly ionized He^+ (30.4 nm) change with altitude at night by utilizing an exospheric sounding rocket. They found that the intensity decreased from 12 to 4 Rayleigh when ascending from 420 to 1200 km. Kumar et al. (1973) firstly measured the 30.4 nm intensity radiation during the daytime, and the intensity was 9.3 ± 3.1 Rayleigh at the height of 186 km. The distribution of partial plas-

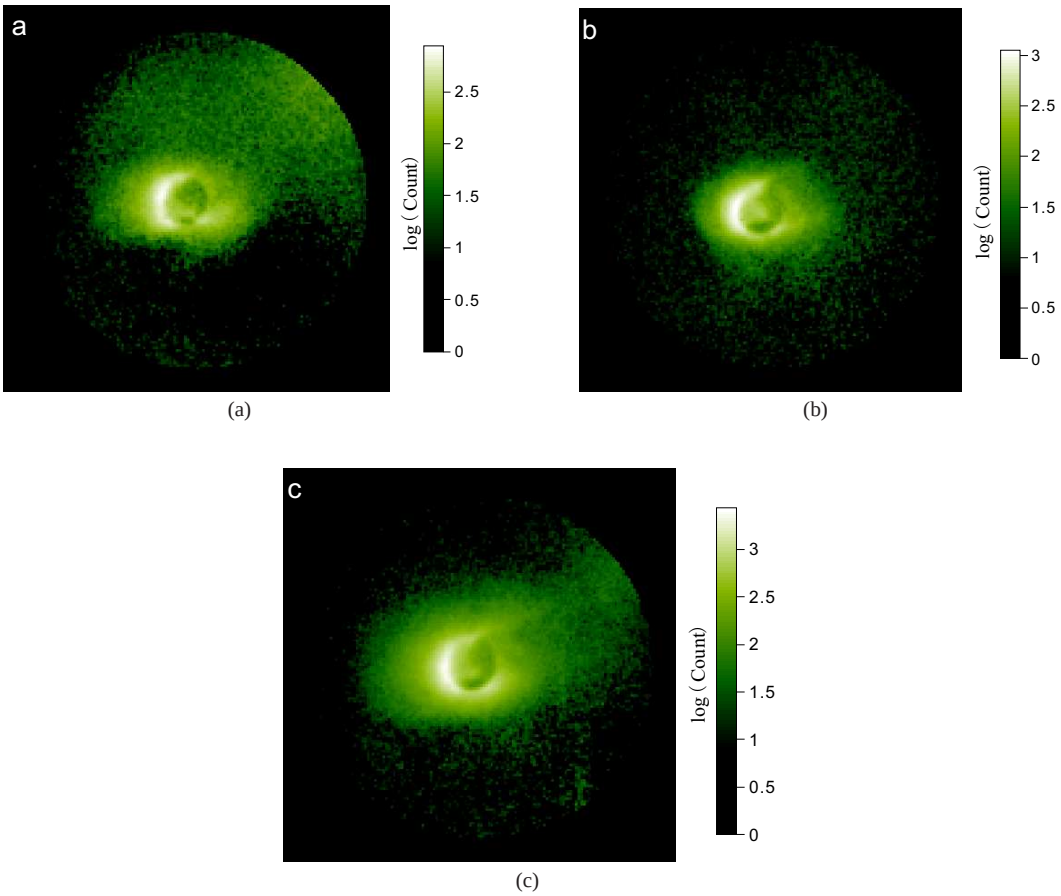

Fig. 6 (a) is an image obtained at 19:23 on 2014 January 22 (UTC time). (b) is an image obtained at 22:30 on 2014 February 21. (c) is an image obtained at 23:58 on 2014 March 22.

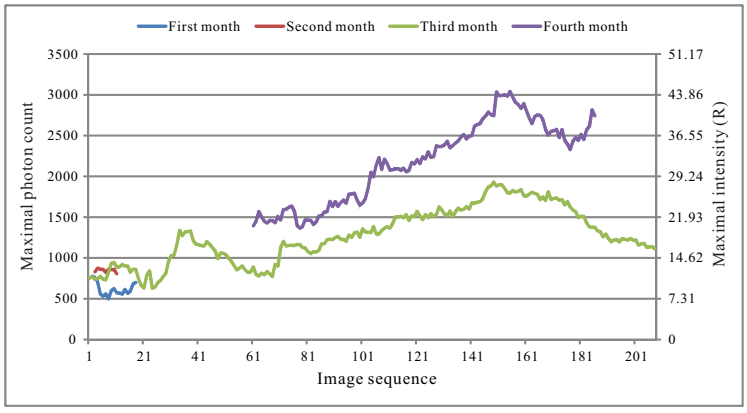

Fig. 7 The statistical results of the maximal photon count and intensity for images (after background removal) obtained in the first four months. The "background" images and severely contaminated images are not included.

maspheric He^+ emission projected on the meridian plane was obtained by the XUV scanner and showed that the maximal intensity was 9 Rayleigh (Nakamura et al. 1999). The images acquired by IMAGE-EUV gave the result that the intensity was $0.1 \sim 7.9$ Rayleigh (Sandel et al. 2003), projected on the equatorial plane. The images taken by TEX had a counting rate between $0.1 \sim 100\,\mathrm{min}^{-1}$ (Murakami et al. 2010; Darrouzet & De Keyser 2013).

He et al. (2010) and He et al. (2013) simulated the emission intensities and global structures of the plasmasphere viewed from the Moon using a dynamic global core plasma model embedded in a TS07 magnetic field model and W05 electric field model. In their simulation, the emission intensity was 0.1 ∼11.4 Rayleigh within the plasmapause and the maximal count of 30.4 nm photons was 1000 after 10 minutes of accumulation, which is similar to the observation of CE-3 EUVC.

The photon count and emission intensity of EUVC images from the first two months are in good agreement with previous observations and simulations. Although some data from the third and fourth months have higher values, the photon count and emission intensity of EUVC images fluctuate in a normal range. This phenomenon is probably caused by the intense 58.4 nm radiation or the auroral oval, which may come into the view of EUVC when the Moon moves into high magnetic latitudes.

6 CONCLUSIONS

The EUVC operated in good condition and obtained a lot of valuable data during the first several months. Through data processing which includes single image extraction, radiometric calibration, distortion calibration, image resampling, dark current correction, image rotation, image clipping, background removal and geometric positioning, the EUVC raw data are converted into images contained in Level 2B data.

The initial results indicate that the plasmaspheric profile and other features can be clearly seen in the images, and the distribution of photons and the intensity are of the same order of magnitude as in previous studies. The data processing method is reasonable and the EUVC images can be used in further analysis to give researchers a new understanding of the plasmasphere.

Acknowledgements We are grateful to the referee's constructive comments and suggestions, which allowed us to substantially improved the manuscript. We also thank the EUVC instrument team for their help in the data processing.

References

Adrian, M. L., Gallagher, D. L., Green, J. L., & Sandel, B. R. 2001, AGU Spring Meeting Abstracts, 32
Brandt, J. C. 1961, ApJ, 134, 975
Burch, J. L. 2000, Space Sci. Rev., 91, 1
Carpenter, D. L. 2004, Rad. Sci. Bull, 308, 13
Chen, B., Song, K.-F., Li, Z.-H., et al. 2014, RAA (Research in Astronomy and Astrophysics), 14, 1654
Craven, P. D., Gallagher, D. L., & Comfort, R. H. 1997, J. Geophys. Res., 102, 2279
Darrouzet, F., & De Keyser, J. 2013, Journal of Atmospheric and Solar-Terrestrial Physics, 99, 53
Gallagher, D. L., Adrian, M. L., & Liemohn, M. W. 2005, Journal of Geophysical Research (Space Physics), 110, A09201
Gruntman, M. A. 1992, Geophys. Res. Lett., 19, 1323
He, F., Zhang, X., Chen, B., & Fok, M.-C. 2010, Science in China Series E: Technological Sciences, 53, 200
He, F., Zhang, X.-X., Chen, B., Fok, M.-C., & Zou, Y.-L. 2013, Journal of Geophysical Research (Space Physics), 118, 7085
Ip, W.-H., Yan, J., Li, C.-L., & Ouyang, Z.-Y., 2014, RAA (Research in Astronomy and Astrophysics), 14, 1511
Jelinsky, P., Vallerga, J. V., & Edelstein, J. 1995, ApJ, 442, 653
Kumar, S., Bowyer, S., & Lampton, M. 1973, J. Geophys. Res., 78, 1107

Meier, R. R. 1991, Space Sci. Rev., 58, 1
Meier, R. R., & Weller, C. S. 1972, J. Geophys. Res., 77, 1190
Murakami, G., Yoshikawa, I., Obana, Y., et al. 2010, Earth, Planets, and Space, 62, e9
Nakamura, M., Yamashita, K., Yoshikawa, I., et al. 1999, Earth, Planets, and Space, 51, 61
Nakamura, M., Yoshikawa, I., Yamazaki, A., et al. 2000, Geophys. Res. Lett., 27, 141
Ogawa, T., & Tohmatsu, T. 1971, J. Geophys. Res., 76, 6136
Sandel, B. R., Broadfoot, A. L., Curtis, C. C., et al. 2000, Space Sci. Rev., 91, 197
Sandel, B. R., King, R. A., Forrester, W. T., et al. 2001, Geophys. Res. Lett., 28, 1439
Sandel, B. R., Goldstein, J., Gallagher, D. L., & Spasojevic, M. 2003, Space Sci. Rev., 109, 25
Yoshikawa, I., Yamazaki, A., Murakami, G., et al. 2008, Earth, Planets, and Space, 60, 407